10.22059/IJVM.2022.335899.1005219

Iranian Journal of Veterinary Medicine
Volume 16- Issue 4

Original Article
Online ISSN: 2252-0554

Fabrication of Platelet-Rich Fibrin-Coated Polycaprolactone/Hydroxyapatite (PCL-HA/PRF) 3D Printed Scaffolds for Bone Tissue Engineering

Sina Yal Beiranvand[1], Hossein Nourani[2], Hossein Kazemi Mehrjerdi[1]*

1. *Department of Clinical Sciences, Faculty of Veterinary Medicine, Ferdowsi University of Mashhad, Mashhad, Iran*
2. *Department of Pathobiology, Faculty of Veterinary Medicine, Ferdowsi University of Mashhad, Mashhad, Iran*

Abstract

BACKGROUND: Tissue engineering is a potential technique for treating bone tissue abnormalities in the short and long terms. Aside from that, the use of 3D printing technology has considerable advantages in the production of bioengineering scaffolds for the treatment of patient-specific bone defects.

OBJECTIVES: The aim of the study was to fabricate and characterize the 3D printed polycaprolactone/hydroxyapatite (PCL-HA) scaffolds modified with Platelet-rich Fibrin (PRF).

METHODS: The scaffolds were fabricated using 3D printing technology to provide a suitable environment for the bone regeneration. Scanning electron microscopy (SEM), Fourier transform infrared (FTIR), and compression tests were utilized to characterize the scaffold morphology, microstructure, and mechanical properties, respectively. The potentials for the cell adhesion, proliferation, biocompatibility, and differentiation were also investigated.

RESULTS: The 3D PCL-HA scaffold with linked pores had a moderately rough surface as a result of hydroxyapatite (HA) nanoparticles incorporation, which resulted in the increased mechanical properties. Increased bone cell proliferation on the PCL-HA/PRF scaffold surface was seen as a result of the enhanced hydrophilicity and porosity of the PCL-HA/PRF scaffold as compared to the PCL scaffold. The MTT assay results showed that the PCL-HA/PRF scaffold was much more cyto-compatible than the PCL and PCL-HA scaffolds, which was a major improvement.

CONCLUSIONS: The results showed that 3D printed PCL-HA scaffold supplemented with Platelet-rich Fibrin (PRF) may be an effective scaffold for the bone tissue regeneration.

KEYWORDS: 3D printing scaffolds, Bone tissue engineering, Hydroxyapatite, Osteogenic differentiation, Platelet-rich Fibrin

Correspondence

Hossein Kazemi Mehrjerdi, Department of Clinical Sciences, Faculty of Veterinary Medicine, Ferdowsi University of Mashhad, Mashhad, Iran Tel: +(51) 3880 5611, Fax: +98 (51) 38803701, Email: h-kazemi@um.ac.ir

Received: 2021-12-19

Accepted: 2022-03-14

How to Cite This Article
Yal Beiranvand , S ., Nourani, H., Kazemi Mehrjerdi, H. (2022). Fabrication of Platelet-Rich Fibrin-Coated Polycaprolactone/Hydroxyapatite (PCL-HA/PRF) 3D Printed Scaffolds for Bone Tissue Engineering. *Iranian Journal of Veterinary Medicine, 16*(4), 400-413.

Introduction

Bone is composed of the collagen fibrils, nano-crystalline, and rod-like inorganic materials with the length ranging from 25 to 50 nm (Ralston, 2021; Maia *et al.*, 2022). The bone tissue abnormalities is a common problem that can be caused by a variety of factors, such as tumors, trauma, congenital malformations, and senile osteoporosis (Tian *et al.*, 2021). The current treatments for the bone abnormalities are ineffective due to the lack of blood vessels in bone tissues, increased operating time, and increased healthcare costs (Venugopal *et al.*, 2019). The development of a suitable method, such as tissue engineering technology, makes it possible to regenerate diseased or damaged tissues, such as bone (Davoodi *et al.*, 2020; Rastegar *et al.*, 2021; Maia *et al.*, 2022).

Over the last few decades, researchers have become more interested in Additive Manufacturing (AM) for creating 3D porous scaffolds for the cell growth (Cestari *et al.*, 2021). Unlike traditional polymer processing techniques like salt leaching and gas foaming, AM can easily be incorporated into the scaffold fabrication with controlled porosity. This enables patients to have exact dimensions of individual artificial bone substitutes (Tian, 2020). Fusion deposition modeling, 3D printing, 3D bio-plotting, stereolithography, and selective laser sintering are all examples of the AM technologies utilized in computer-aided tissue engineering (Hassanajili *et al.*, 2019).

Various biomaterials are combined with advanced technologies to create bone structures that resemble those found in the body. Biomaterials used in the tissue engineering may help restore damaged body functions, as well as provide structure for the cell specialization, migration, and proliferation (Shrivats, Mcdermott and Hollinger, 2014). The scaffold supports cell growth, cell function, and the formation of the extracellular matrix (ECM) in the body (Cakmak *et al.*, 2020).

Bone is mainly composed of calcium phosphate (58%), calcium carbonate (7%), calcium fluoride (14%), magnesium phosphate (14%), and sodium chloride (1%). These minerals combine to form hydroxyapatite (Shor, 2007). Hydroxyapatite (HA; $Ca_{10}(PO_4)_6(OH)_2$) is a biomaterial with chemical and crystallographic properties similar to the natural bone (Kattimani, Kondaka and Lingamaneni, 2016; Mojahedian *et al.*, 2016; Chatzipetros *et al.*, 2018). Studies have shown it has a promising synthetic scaffold for the bone regeneration (Biazar *et al.*, 2020; Bigham-Sadegh *et al.*, 2020; Ramesh *et al.*, 2020; Souza *et al.*, 2020; Bastami, Semyari and Tabrizi, 2021). However, it has poor biomechanical properties such as brittleness, fatigue strength, and flexibility. The material is therefore unsuitable for the direct loading and dynamic force applications in *in vitro* bone tissue engineering (Chuenjitkuntaworn *et al.*, 2010; Maia *et al.*, 2022).

Poly Ɛ-caprolactone (PCL), Known for its biocompatibility and biodegradability, has been used in conjunction with HA derived from the biological sources to form 3D printed scaffolds for bone regeneration (Kattimani, Kondaka and Lingamaneni, 2016; Cakmak *et al.*, 2020; Cestari *et al.*, 2021). Moreover, PCL is one of the most hydrophobic commercially available biodegradable polymers, with acceptable mechanical properties. It is very compatible with a wide range of other types of polymers, allowing it to be used in a wider range of applications (Sahebalzamani, Khorasani and Joupari, 2017; Dwivedi *et al.*, 2020).

Platelet-rich fibrin (PRF) is a Fibrin-based material derived from blood discovered by Choukroun in 2000 (Simonpieri *et al.*, 2009). PRF was originally intended for and used in oral and maxillofacial surgery, particularly sinus lifts (Mazor, Choukroun and Toffler, 2009; Choukroun *et al.*, 2006; Simonpieri *et al.*, 2009), but it has also been used in middle ear surgery and peri-implant defect filling (Jang *et al.*, 2010). PRF is obtained by centrifugation of the patient's blood in the absence of an anticoagulant, which causes platelet entrapment in fibrin clots in the centrifugation tube (Douglas *et al.*, 2012).

The current study used 3D printing technique to create a PCL-HA/PRF composite scaffold. The FTIR analysis was used to compare the composite scaffold and 3D printed PCL to understand the chemical bonding. The compression test was used to assess the materials mechanical properties. The adhesion, proliferation, biocompatibility, and

differentiation properties of the 3D scaffold on the cells were also studied *in vitro* using osteoblasts.

Materials and Methods

Preparation of PCL-HA Composite

PCL (Poly Ɛ-caprolactone, Sigma-Aldrich) granules (15 g) (5% w/v) were dissolved in DCM (Dichloromethane, Sigma-Aldrich) and stirred vigorously for 2 h at 70°C until the solution was homogenized. Following that, HA nanoparticles (Hydroxyapatite, Pardis Pajoohesh, Co, Iran, particle size <20 nm) were added to the solution (HA: PCL volume ratio of 1:4), and stirred for 1 h at 60°C until a milky suspension was obtained. The solution was placed into a petri dish and allowed to dry. The resulting composite film was then sliced into pellets about 0.5 mm^2 in size. Similarly, to the control sample, pure PCL was dissolved in DCM and subjected to the same treatment.

Fabrication of 3D Printed Scaffolds

Porous PCL-HA scaffold was designed and then constructed using a BioFabX2 machine manufactured by Omid Afarinan Co., Iran. First, a scaffold with a rectangular base was designed using the CAD software Solidworks. The pore size of 900 µm was chosen for this application. The layer height was decided to be 500 µm to ensure the best possible deposition and adhesion between neighboring layers. In order to feed the material from a heated chamber to a flow nozzle, which was optimized before, it is necessary to employ compressed air. The PCL-HA pellets were loaded into the cartridge, which was pre-heated to the desired temperature and held for 15 min before the process to ensure homogeneity of the melt during the subsequent procedure. The nozzle inner diameter was 500 µm. To achieve the best results, the printing pressure and the speed were 6 bar and 2 mm/s, respectively. The temperature in the chamber was set to 90°C. The same process was used to build the 3D printed PCL scaffold that was served as a control for the experiment.

Platelet-rich Fibrin Preparation

The Choukroun method was used to create the PRF (Simonpieri *et al.*, 2009). For this purpose, 10 mL of human blood was placed into a test tube with no coagulant agent and centrifuged (Zenithlab-LC-04C) for 3 minutes at 700 rpm. The resulting PRF solution was drawn out of the test tube center and PCL-HA scaffold was immersed in it. Once the fluid was sucked out, the PCL-HA/PRF scaffold was vacuum dried. The procedures outlined above were repeated three times for the following experiments.

Characterization of the 3D Printed Scaffolds Scaffolds Morphology

The morphology of the PCL and PCL-HA scaffolds was observed using Field emission scanning electron microscopy (FESEM, MIRA3 TESCAN). The mean thickness of the strands and the pore sizes were measured by a computed image analyzer (Image J, 1.48v). All samples were sputter-coated with gold prior to the FESEM test.

Fourier Transform Infrared (FTIR) Spectroscopy

The FTIR spectroscopy (BRUKER-TENSOR27) was used to determine the bands between the ceramic and polymer phases in the composite material and to identify the functional groups of PCL, HA, and PRF. The samples were ground with potassium bromide (KBr), and the FTIR spectrum was analyzed in the range of 500-4000 cm^{-1}.

Water Contact Angle

The wettability of PCL and PCL-HA/PRF scaffolds was determined using a contact angle goniometer (OCA 50, Dataphysics, Germany). Deionized water (20 µL) was dripped onto the surface of each scaffold, and then a high-resolution camera was used. Calculating the contact angle value was done by taking the average of five separate locations on the scaffolds.

Mechanical Compression Test

The mechanical properties of the samples were measured using a compression strength instrument (AG-X Plus, Shimadzu Co.). The prepared specimens (n=3) from each group of PCL, PCL-HA, and PCL-HA/PRF scaffolds were cut into 10×10×5 mm^3. The tests were performed at a strain rate of 1 mm min^{-1}, between two steel platen members.

In Vitro Biological Assay

Cell Culture

The osteoblast-like cells, MC3T3-E1 (NCBI C555, Pasteur Institute, Iran) were cultured in Dulbecco's Modified Eagle Medium F-12 (DMEM/F-12) at 37°C and 100% humidity with 5% CO_2. The

medium was enriched with 10% fetal bovine serum (FBS) and 1% penicillin/streptomycin.

Cell Morphology Evaluation

The PCL, PCL-HA, and PCL-HA/PRF scaffolds were all trimmed to the appropriate size for the procedures. On each scaffold, roughly 2×10^4 cells were seeded with 10% FBS in DMEM/F-12. After 24 h, the cell-scaffold formations were taken from the culture fluid and washed with PBS before being fixed for 2 h with 2.5% glutaraldehyde (Sigma-Aldrich) and dehydrated with graded ethanol. The samples were subsequently coated with gold and inspected under a scanning electron microscope.

Cell Viability

The MTT assay was used to examine the cell viability on the surfaces of the PCL, PCL-HA, and PCL-HA/PRF scaffolds. In order to prepare for the MTT test, the scaffolds were sliced into 10×10 mm^2. The scaffolds were exposed to 25 kGy gamma radiation for five days in order to be disinfected. The cells were seeded in 24-well plate (5×10^5 cells/well) in 100 µL of media on the sterilized scaffolds and allowed to incubate for 24 h. Three wells containing MC3T3-E1 cells were used as control samples with no scaffold. Incubation was completed for 4 h after the culture medium was taken from each well. After one day, the culture medium was removed from each well and 500 µL of MTT (0.5 mg mL^{-1}) was applied to each well, followed by 4 h incubation. Then, Dimethyl sulfoxide (DMSO, Sigma-Aldrich) was used to dissolve the purple-colored crystals that had formed in each well. The plate was shaken for 15 min in order to obtain a better solution. Afterwards, the optical density (OD) of living cells was determined with an ELISA reader operating at 570 nm (Avecina, Pishtaz teb, Iran). In the end, the percentage of viable cells on each scaffold was calculated using the following formula:

$$\%\ Cell\ Viability = \frac{OD\ sample}{OD\ control} \times 100$$

Cell Proliferation

The MC3T3-E1 cells were seeded in 24-well culture plates (2×10^5 cells/well) into each scaffold with DMEM/F-12 medium plus 10% FBS and cultured at 37°C in a humidified incubator with 5% CO_2. The scaffolds were removed from the media at days 1, 3, and 7 and washed twice with a buffer solution. In order to count the number of proliferated cells, a Cell Counting Kit-8 (CCK-8, Vazyme) was used. For the most part, the CCK-8 solution was diluted with culture media (1:10) before being administered to each individual sample. It was necessary to extract the CCK-8 suspension and transfer it to 96-well plates after four hours of incubation. The OD of the extracted suspension was determined at 570 nm using an ELISA reader (BioTec ELx 800, USA).

Real time-PCR

The RT-PCR was used to determine the levels of osteogenesis-related gene expression in MC3T3-E1 cells that had been grown on various scaffolds for 14 and 21 days. Total RNA was isolated from the cells using the TRIzol Reagent (DNAbiotech), and reverse transcription PCR was carried out using the SuperRT cDNA Synthesis Kit (DNAbiotech) according to the manufacturer's instructions. The levels of osteogenic markers were determined using an UltraSYBR Mixture (DNAbiotech). For the relative real-time PCR, the primer sequences for the target gene and the internal control gene (glyceraldehyde-3-phosphate dehydrogenase (GAPDH)) were as follows: OCN (F:5′-CCGGGAGCAGTGTGAGCTTA-3′; R:5′-AGGCGGTCTTCAAGCCATACT-3′), Runx2 (F:5′-TTCTCCAACCCACGAATGCAC-3′; R:5′-CAGGTACGTGTGGTAGTGAGT-3′); GAPDH (F:5′-GACTTCAACAGCAACTCCCAC-3′; R:5′-TCCACCACCCTGTTGCTGTA-3′). The findings of the RT-PCR experiments were analyzed by $2^{-\Delta\Delta Ct}$ method, and all data were normalized to the level of GAPDH expression.

Alizarin Red Staining (ARS)

The MC3T3-E1 cells were seeded in 24-well culture plates (2×10^5 cell/well) and incubated overnight at 37°C in a humidified incubator with 5% CO_2. After that, the media was changed to Osteocyte Differentiation medium for a total of 19 days. The cells were then fixed in 70% ethanol for 1 hr at 4°C before being processed. The cells were rinsed with PBS and then stained with 1% (w/v) ARS, pH 4.2, for 10 min at room temperature. The production of mineralized matrix was then found to take place after that. The scaffolds in the blank control group were completely devoid of the cells. The amount of ARS

staining was measured by elution with 10% (w/v) cetylpyridinium chloride (Sigma-Aldrich), which was applied for 30 min at room temperature, and the OD was measured at 405 nm.

Results

Morphology of the Scaffolds

The SEM images of the 3D scaffolds taken from the top perspective are shown in Figure 1. The thickness of the strands and the pore sizes are summarized in Table 1. In contrast to the strands of pure PCL scaffold, which have an average thickness of 431 µm, strands of the PCL-HA scaffold showed a higher average length of 545 µm. Consequently, the average pore size in the PCL-HA scaffold was greater (901 µm). A few micropores could be detected on the surface of all the scaffolds, although they were concentrated on the strands of the PCL-HA scaffolds than on the surface of the others. The diameter of these micropores was less than 10 µm.

As illustrated in Figure 1, the presence of HA particles can be readily seen in all SEM images of the scaffolds (d). The EDX is used to examine the particles and it appears that they are clustered in 10-20 µm clusters that are otherwise homogeneously disseminated inside the PCL matrix (Figure 1 e-h). The presence of the HA constituents was confirmed by EDX.

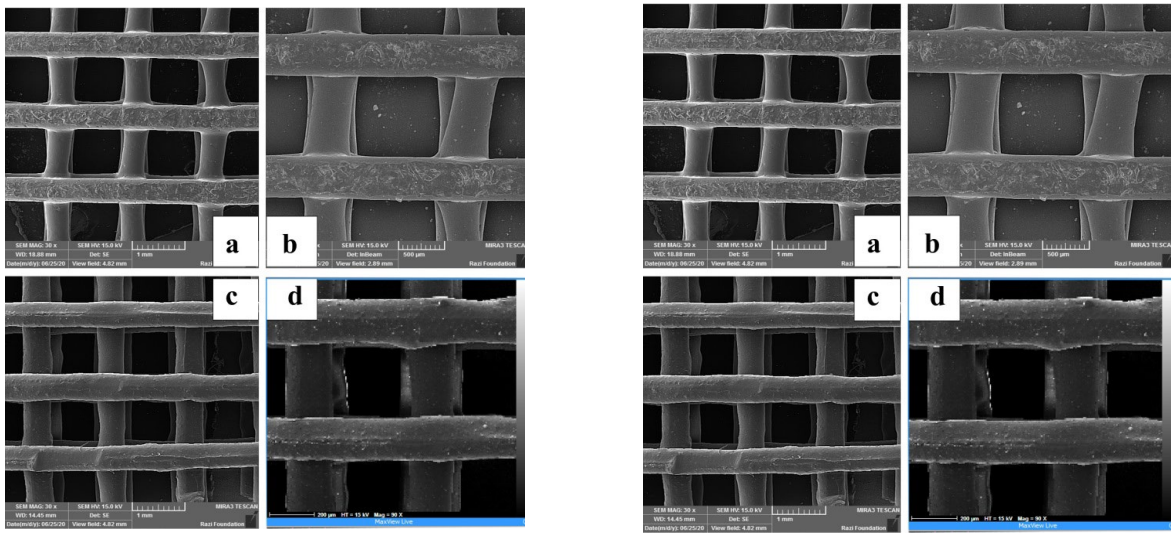

Figure 1. The FESEM images of the 3D printed scaffolds (top view). (a, b) PCL scaffolds, (c, d) PCL/HA scaffolds, (e-h) PCL/HA scaffold elemental mapping analysis.

Table 1. Dimensions of 3D printed scaffolds.

	PCL	PCL-HA
Strand thickness (µm)	431±24	545±31
Pore size (µm)	900±11	901±80

FTIR Results

The FTIR spectroscopy was used to identify the functional groups in pure polymers and their composites. The FTIR spectra of the PCL, PCL-HA, and PCL/PRF scaffolds detected in the 400–4000 cm^{-1} range are presented in Figure 2. The absorption peaks of 2920 cm^{-1}, 2860 cm^{-1}, 1635 cm^{-1}, and 1160 cm^{-1} in the PCL were corresponded to the CH_2 symmetric stretch, CH_2 asymmetric stretch, carbonyl stretch, and C-O stretch, respectively. The peak at 1157 cm^{-1} was attributed to the phosphate group in HA, which overlapped with the C=O band in PCL. Furthermore, PRF bands at 3260 and 1524 cm^{-1} belong to the NH groups (amide II), respectively.

Contact Angle Results

The static contact angles of the PCL and PCL-HA/PRF scaffolds are shown in Figure 2 b. The PCL scaffold had a static contact angle of 90.66±2.90°. As compared to the PCL scaffold surface, the contact angle of the PCL-HA/PRF scaffold surface showed a significant reduction, which was dramatically lowered to 15.50±1.57°.

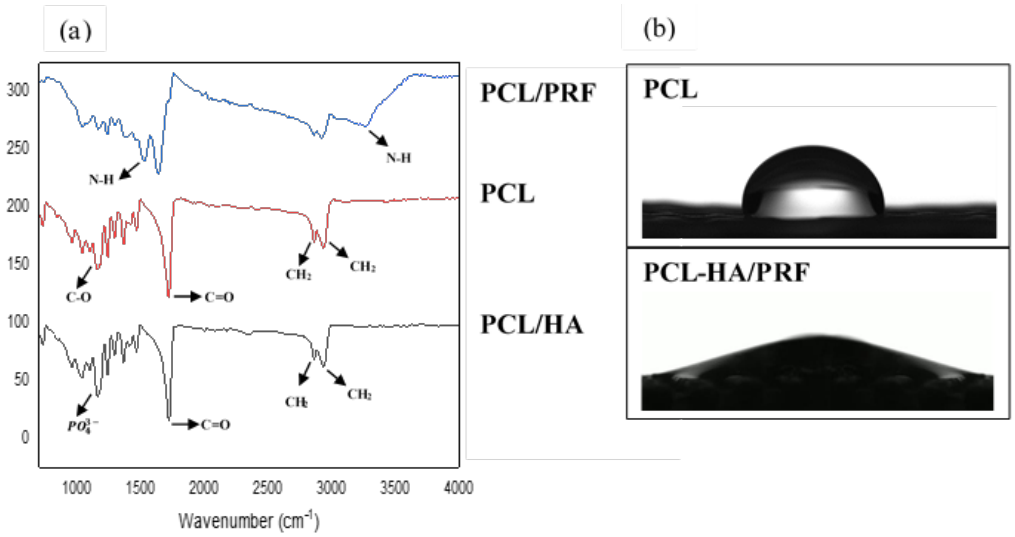

Figure 2. (a) FTIR spectrum of the PCL/PRF, PCL, and PCL/HA scaffolds. (b) Static contact angles of the PCL and PCL-HA/PRF scaffolds.

Compression Test Results

Figure 3 shows the results of the compression properties evaluation. The compressive modulus of the PCL-HA scaffold was 67.04±39.67 MPa, whereas the compressive modulus of the PCL scaffold was 66.17±21.76 MPa, indicating a significant difference in the strength, as shown in Figure 3 b.

In vitro Biological Assay Results

Cell Attachment and Cell Viability Results

The SEM micrographs of morphological characteristics of MC3T3-E1 cells cultured for 2 and 3 weeks on the PCL, PCL-HA, and PCL-HA/PRF scaffolds are demonstrated in Figure 4. To assess the biocompatibility of the scaffolds, MC3T3-E1 cells were used as a cell model. The MC3T3-E1 cells were seeded on the scaffold surfaces. MTT assay and optical density analysis were used to assess the viability of the cells on the scaffold surface. Figure 5 depicts the viability of MC3T3-E1 cells on the surfaces of PCL, PCL-HA, PCL-HA/PRF scaffolds, and control sample. On day 1, cell viability was 81%, 87%, and 121% for the PCL, PCL-HA, and PCL-HA/PRF scaffolds, respectively.

Cell Proliferation Results

The MC3T3-E1 cells were cultured on the PCL, PCL-HA, and PCL-HA/PRF scaffolds to determine their proliferation. The CCK-8 test was conducted to determine the proliferation of the cells (Figure 6). The optical density of the CCK-8 solution was measured after the cells were seeded at various time intervals.

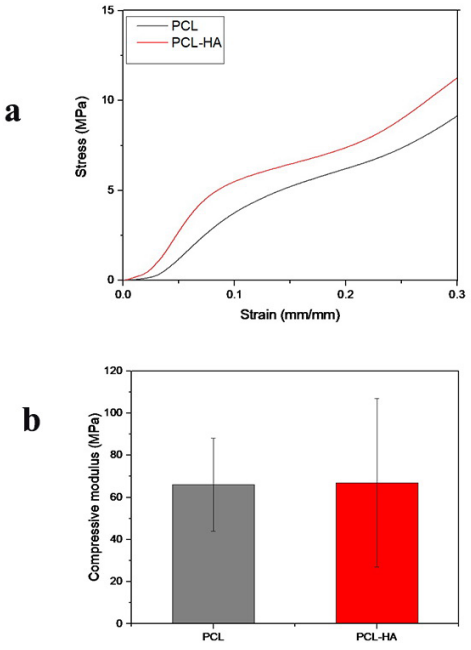

Figure 3. (a) Stress-strain curves of PCL and PCL-HA scaffolds. (b) Compressive modulus of PCL and PCL/HA scaffolds.

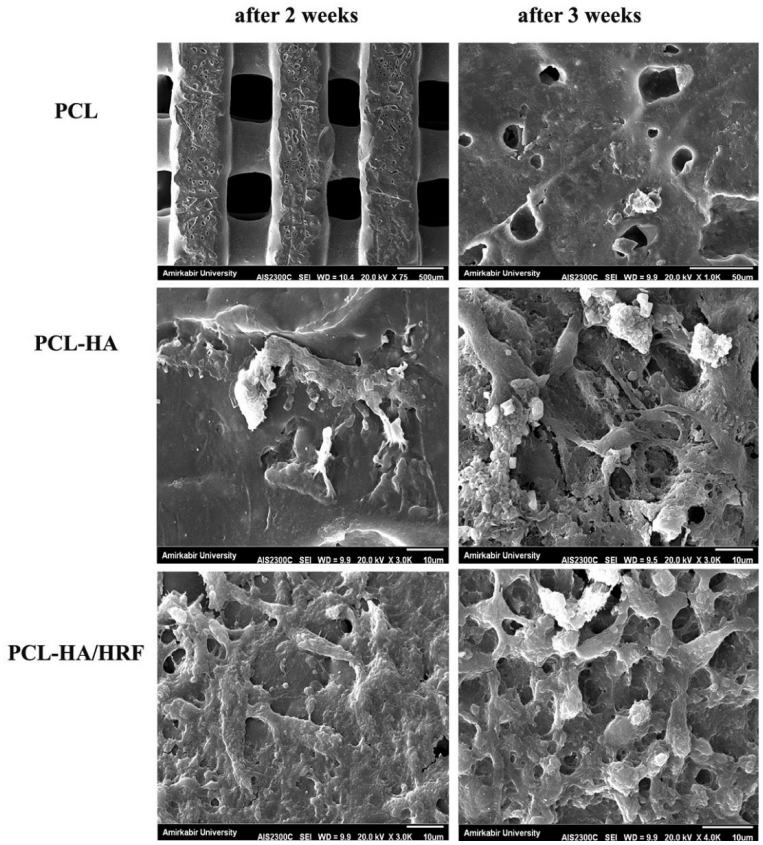

Figure 4. SEM images of MC3T3-E1 cells cultured on the PCL, PCL-HA, and PCL-HA/PRF scaffolds.

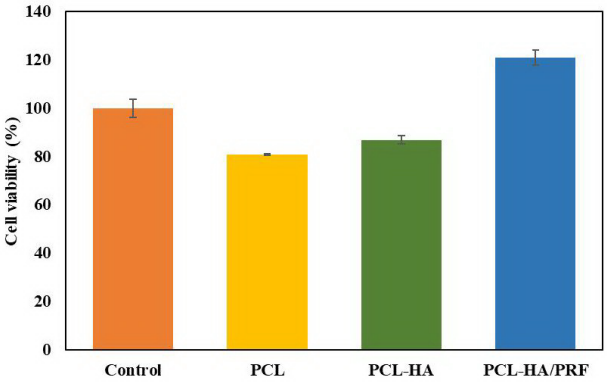

Figure 5. Cell viability of MC3T3-E1 cells seeded on the PCL, PCL-HA, PCL-HA/PRF scaffolds, and control sample on day 1 of culture.

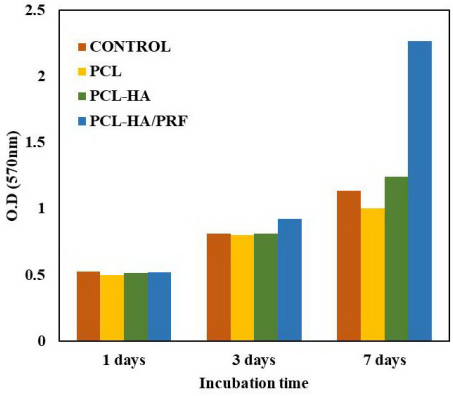

Figure 6. Proliferation of MC3T3-E1 cells on the scaffolds.

Real time-PCR Results

RT-PCR was employed to evaluate the expression of the genes involved in osteogenesis (Runx2 and OCN) in the cells cultured for 2 and 3 weeks. Comparing the PCL, PCL-HA, and PCL-HA/PRF scaffolds to the control sample, upregulation of the Runx2 and OCN genes expression was identified in the PCL and PCL-HA/PRF scaffolds, as illustrated in Figure 7. As compared to the PCL-HA/PRF scaffold, the changes in Runx2 and OCN genes expression caused by the PCL-HA scaffold were minor.

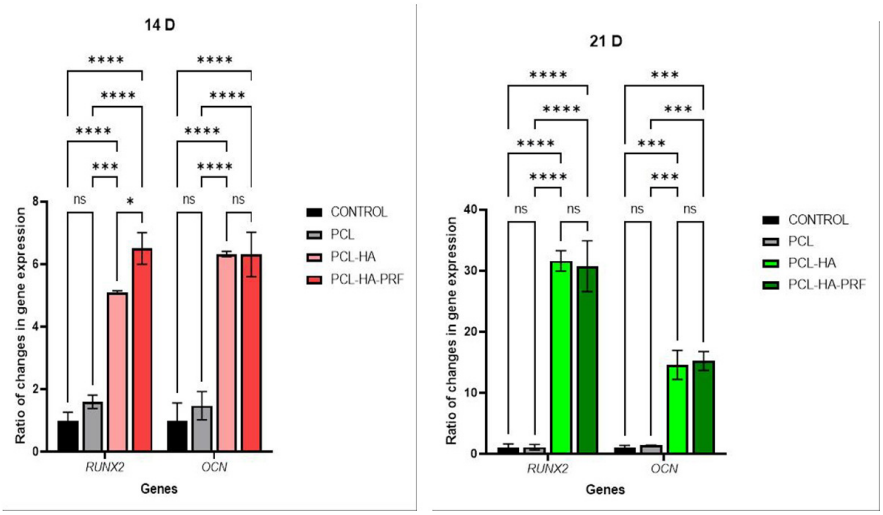

Figure 7. Relative assessment of osteogenesis-related genes expressions (Runx2, and OCN) in (a) 14 days, and (b) 21 days.

Alizarin Red Staining Results

Alizarin-Red staining is used to identify calcium-containing osteocytes in differentiated culture of mesenchymal stem cells (MSCs). Following incubation of the MC3T3-E1/scaffold composite in Osteocyte Differentiation medium for 14 and 21 days, more noticeable positive staining was observed on PCL-HA and PCL-HA/PRF scaffolds (Figures 8 b-c) than on PCL scaffold (Figure 8 a).

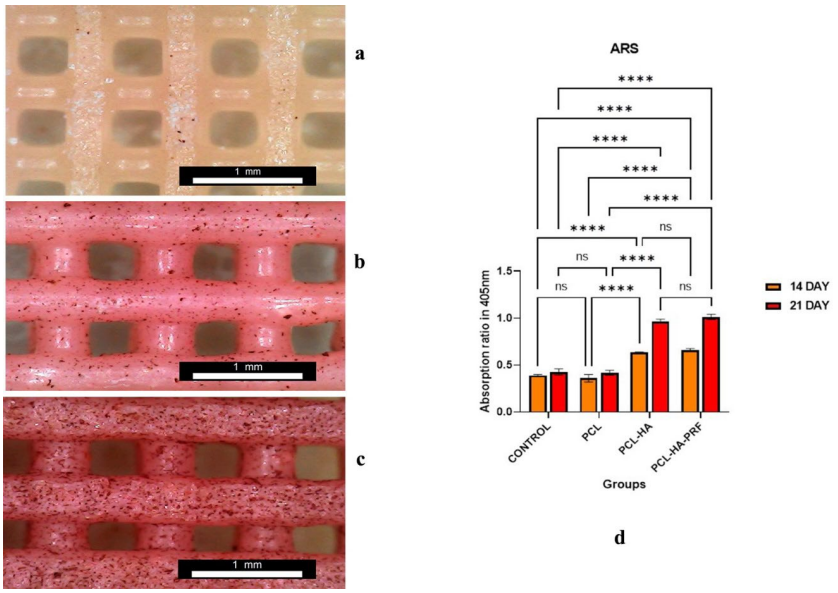

Figure 8. Alizarin Red staining of MC3T3-E1 cells on the scaffolds ((a) PCL, (b) PCL-HA, (c) PCL-HA/PRF). (d) ARS quantification of mineral content.

Discussion

In accordance with the results of SEM images depicted in Figure 1, the strands in the pure PCL-HA scaffold were larger than those in the PCL scaffold, resulting in an increase in the average pore size in the PCL-HA scaffold. Given that the printing speed and air pressure were both set to the same value for all materials, it is assumed that the thickness of the strands will be governed only by the viscosity of the material used in the printing. The viscosity should decrease with increasing temperature and increase

with an increase in the ceramic filler concentration and specific surface area (Hanemann, 2008). If the temperature of all scaffolds is maintained at the same level, the variance in the strand thickness is related to the presence of ceramic filler in some scaffolds. This could explain why the PCL-HA scaffold has larger material flow strands than the PCL scaffold, yet the PCL scaffold has thicker material flow strands. Furthermore, few micropores discovered on the surface of all scaffolds are expected to increase cell-scaffold interactions that are advantageous to the osteogenesis. Moreover, the macropores formed by the 3D printing process should allow cells to penetrate and stimulate vascularization while also boosting osteogenesis (Riches *et al.*, 2017). The presence of HA particles on the scaffolds surfaces also results in roughness on the surface of the material, which may have an effect on the cell adherence.

According to the results of FTIR spectroscopy shown in Figure 2 (a), the bands of HA and PCL in the spectrum, confirmed the formation of both compounds in the 3D printed scaffold. The C=O, CO, and C-H bands were found to be associated with PCL, whereas the PO_4^{3-} band was found to be associated with HA. As a result of the formation of chemical bonds between HA and PCL during the chemical process, minor displacements of HA-PCL nanocomposite peaks have occurred in comparison with pure PCL peaks, which are negligible. The FTIR spectra of 3D printed scaffolds revealed that all the constituents preserved their chemical structures after completion of the production process.

When compared to the PCL scaffold, the contact angle of the PCL-HA/PRF scaffold surface was dramatically lowered to a significant reduction to 15.50±1.57°. As a general rule, hydrophilic surfaces have contact angles that range from 0° to 30°, and less hydrophilic surfaces have contact angles that range from 0° to 90°. Those materials that have a contact angle greater than 90° are considered hydrophobic (Shalumon *et al.*, 2011). The results showed that the addition of PRF to the PCL-HA/PRF scaffold resulted in a considerable increase in the hydrophilicity of the scaffold.

Figure 3 shows the results of the compression properties. As can be observed, the stress-strain curves for the scaffolds went through three stages. During the initial stage, linear behavior could be observed, which was associated with the elastic response. The second step, characterized by practically constant tension, was corresponded to the collapse of pores under pressure, while the third step was linked to the densification of the scaffold. The compression modulus is defined as the slope of the linear component of the stress-strain curve during the stress-strain period. According to the results of the compressive modulus tests, the compressive modulus of the PCL-HA scaffold was higher than that of the PCL scaffold. The enhanced compressive modulus of the PCL-HA scaffold revealed that the addition of HA particles resulted in improved mechanical properties. It is possible that bone healing scaffolds will be subjected to the severe mechanical stress after implantation. Therefore, the mechanical properties of the scaffolds must be taken into consideration. According to the reports, HA functions as a support and filler in bone, and it has the potential to become a permanent part of the bone skeleton (Salmoria *et al.*, 2013).

The morphological properties of MC3T3-E1 cells cultured for 2 and 3 weeks on the PCL, PCL-HA, and PCL-HA/PRF scaffolds were revealed by SEM (Figure 4). The surfaces of the PCL-HA and PCL-HA/PRF scaffolds were found to have more cells adhesion than the surfaces of the PCL scaffolds. The interactions between cells were established in the pores of both the PCL-HA and the PCL-HA/PRF scaffolds, with the PCL-HA/PRF scaffold demonstrating the most dramatic effect of the two scaffolds. On PCL-HA and PCL-HA/PRF scaffolds, cell adhesion and extension were observed to be great, however, cells did not disseminate entirely on the PCL scaffolds.

The viability of MC3T3-E1 cells was determined on the surfaces of PCL, PCL-HA, PCL-HA/PRF scaffolds, as well as on the surface of the control sample. The cell viability in the PCL-HA/PRF scaffold was significantly higher than in the PCL-HA scaffold and the control sample. There was, however, no statistically significant difference between the PCL-HA scaffold and the PCL scaffold. As a result, the effect of PRF on cytotoxicity of the scaffold may be less than the effect of HA.

According to the proliferation assay results, the OD values of the PCL-HA/PRF scaffold were statistically higher than those of the PCL and PCL-HA scaffolds, and those of the PCL/HA scaffolds were significantly higher than those of the pure PCL scaffolds, indicating that cell proliferation on the PCL-HA/PRF scaffolds was better than that on the PCL and PCL-HA scaffolds. When compared to the smooth surfaces, rough surfaces frequently promote the adhesion and proliferation of a variety of cell types (Shim, Huh and Park, 2013). Because of the roughness of the strand surface, the surface area of the scaffold can be increased, which in turn improves its hydrophilicity (Ma *et al.*, 2017). We discovered that the strands of PCL-HA and PCL-HA/PRF scaffolds had a fairly rough surface when examined under high magnification SEM (Figure 1 (b, d, and f), whereas the PCL scaffold had a smooth surface. Figure 4 shows the MC3T3-E1 cells with longer pseudopodia spread more readily on the PCL-HA and PCL-HA/PRF scaffolds than on the PCL scaffolds, suggesting that the moderately rough surfaces of PCL-HA and PCL-HA/PRF scaffolds facilitated more cell attachment and proliferation.

According to the researches, more hydrophilic surfaces were more suitable for the cell adhesion, migration, and proliferation than their hydrophobic counterparts (Wei *et al.*, 2006). Furthermore, the hydrophilicity facilitates in the absorption of fibronectin is essential for the osteoblast adhesion *in vitro* (Yang *et al.*, 2004). The static contact angle of the PCL-HA/PRF scaffolds was significantly lower than that of the PCL scaffold (Figure 2 b). Thus, the PCL-HA/PRF scaffold was shown to be the most advantageous for the cell adhesion and proliferation in our investigation.

The changes in Runx2 and OCN genes expression caused by the PCL-HA scaffolds were minor compared to the PCL-HA/PRF scaffolds (Figure 7). According to Maruyama and colleagues, Runx2 null mice did not develop any bone formation, showing that Runx2 is a transcription factor that is essential for the osteoblast development (Maruyama *et al.*, 2007). In the post-proliferative period, OCN is expressed at a high level, which is reached during mineralization, and accumulates in the mineralized bone (Liu, Zhang and Li, 2012). According to our findings, the addition of HA particles caused high levels of Runx2 and OCN expression in MC3T3-E1 cells cultured on the PCL-HA or PCL-HA/PRF scaffolds, hence encouraging the process of osteoblast differentiation and bone production. HA in composite materials has been shown in several investigations to be able to trigger osteogenesis (Frohbergh *et al.*, 2014). Furthermore, the relatively rough surface of the scaffolds may enhance the differentiation of MC3T3-E1 cells into osteoblasts. Thus, materials with a moderately rough surface have the ability to stimulate osteogenic genes expression and osteogenic differentiation in human bone marrow-derived mesenchymal stromal cells (hMSCs) (Wall *et al.*, 2009). The results showed that the surfaces of the PCL-HA and PCL-HA/PRF scaffolds were relatively rough, which might result in a high level of osteogenic differentiation and mineralization in the treated areas.

The production of mineralized nodules is a phenotypic marker for the final stage of the mature osteoblast development (Tian, 2020). After 14 and 21 days of incubation in Osteocyte Differentiation medium with MC3T3-E1/scaffold composite, more noticeable positive staining of Alizarin Red was found on PCL-HA and PCL-HA/PRF scaffolds (Figures 8 b-c) than on PCL scaffolds (Figure 8 a). Alizarin Red staining and quantitative analyses (Figure 8 d) revealed that mineralization of the PCL and PCL-HA scaffolds was significantly lower than that of PCL-HA/PRF scaffold, and that mineralization of PCL scaffolds was significantly lower than that of PCL-HA scaffolds. The results of Alizarin Red staining of PCL, PCL-HA, and PCL-HA/PRF scaffolds were found to be completely consistent with the trends observed in the cell proliferation and differentiation during the experiment. The Alizarin Red staining results also revealed that the osteogenic capabilities of the scaffolds were greatly altered by the presence of a PRF coating on the PCL-HA scaffold.

Conclusion

The 3D printed PCL-HA scaffold was modified with Platelet-rich Fibrin (PRF) to create a new PCL-HA/PRF composite scaffold that was found to promote improved bone regeneration and accelerated osteogenic proliferation in the patients undergoing

patient-specific bone abnormality treatments. The scaffolds were found to be cyto-compatible and capable of osteogenic differentiation *in vitro*, which is advantageous not only for the bone regeneration, but also for reducing or preventing the risk of rejection complications in the reparative bone formation, which is beneficial for the bone regeneration. It is necessary to do additional research to discover whether the current scaffolds enable functional tissue regeneration *in vivo*.

Acknowledgments

This study received financial support in the form of Research Project No. 53715 from research council of Ferdowsi University of Mashhad, Mashhad, Iran. We would like to thank all the colleagues for their corporations.

Conflict of Interest

The authors declared no conflict of interest.

References

Bastami, F., Noori-Kooshki, M. H., Semyari, H., Tabrizi, R., Abrishamchian, A., Mashhadi-Abbas, F., ... & Seifalian, A. (2021). Multi-walled carbon nanotube/hydroxyapatite nanocomposite with leukocyte-and platelet-rich fibrin for bone regeneration in sheep model. *Oral and Maxillofacial Surgery*, 1-10. [DOI:10.1007/s10006-020-00933-9] [PMID]

Biazar, E., Daliri J, M., Heidari K, S., Navayee A, D., Kamalvand, M., Sahebalzamani, M., ... & Farajpour L, F. (2020). Characterization and biocompatibility of hydroxyapatite nanoparticles extracted from fish bone. *Journal of Bioengineering Research, 2*(2), 10-19.

Bigham-Sadegh, A., Torkestani, H. S., Sharifi, S., & Shirian, S. (2020). Effects of concurrent use of royal jelly with hydroxyapatite on bone healing in rabbit model: radiological and histopathological evaluation. *Heliyon, 6*(7), e04547. [DOI:10.1016/j.heliyon.2020.e04547] [PMID] [PMCID]

Cakmak, A. M., Unal, S., Sahin, A., Oktar, F. N., Sengor, M., Ekren, N., ... & Kalaskar, D. M. (2020). 3D printed polycaprolactone/gelatin/bacterial cellulose/hydroxyapatite composite scaffold for bone tissue engineering. *Polymers, 12*(9), 1962. [DOI:10.3390/polym12091962] [PMID] [PMCID]

Cestari, F., Petretta, M., Yang, Y., Motta, A., Grigolo, B., & Sglavo, V. M. (2021). 3D printing of PCL/nano-hydroxyapatite scaffolds derived from biogenic sources for bone tissue engineering. *Sustainable Materials and Technologies, 29*, e00318. [DOI:10.1016/j.susmat.2021.e00318]

Chatzipetros, E., Christopoulos, P., Donta, C., Tosios, K. I., Tsiambas, E., Tsiourvas, D., ... & Tsiklakis, K. (2018). Application of nano-hydroxyapatite/chitosan scaffolds on rat calvarial critical-sized defects: A pilot study. *Medicina Oral, Patologia Oral y Cirugia Bucal, 23*(5), e625. [DOI:10.4317/medoral.22455] [PMID] [PMCID]

Choukroun, J., Diss, A., Simonpieri, A., Girard, M. O., Schoeffler, C., Dohan, S. L., ... & Dohan, D. M. (2006). Platelet-rich fibrin (PRF): a second-generation platelet concentrate. Part V: histologic evaluations of PRF effects on bone allograft maturation in sinus lift. *Oral Surgery, Oral Medicine, Oral Pathology, Oral Radiology, and Endodontology, 101*(3), 299-303. [DOI:10.1016/j.tripleo.2005.07.012] [PMID]

Chuenjitkuntaworn, B., Inrung, W., Damrongsri, D., Mekaapiruk, K., Supaphol, P., & Pavasant, P. (2010). Polycaprolactone/hydroxyapatite composite scaffolds: preparation, characterization, and in vitro and in vivo biological responses of human primary bone cells. Journal of Biomedical Materials Research Part A: An Official Journal of The Society for Biomaterials, *The Japanese Society for Biomaterials, and The Australian Society for Biomaterials and the Korean Society for Biomaterials, 94*(1), 241-251. [PMID] [DOI:10.1002/jbm.a.32657.]

Davoodi, A., Zadeh, H. H., Joupari, M. D., Sahebalzamani, M. A., Khani, M. R., & Shahabi, S. (2020). Physico-chemical-and biocompatibility of oxygen and nitrogen plasma treatment using a PLA scaffold. *AIP Advances, 10*(12), 125205. [DOI:10.1063/5.0022306]

Douglas, T. E., Gassling, V., Declercq, H. A., Purcz, N., Pamula, E., Haugen, H. J., ... & Leeuwenburgh, S. C. (2012). Enzymatically induced mineralization of platelet-rich fibrin. *Journal of Biomedical Materials Research Part A, 100*(5), 1335-1346. [DOI:10.1002/jbm.a.34073] [PMID]

Dwivedi, R., Kumar, S., Pandey, R., Mahajan, A., Nandana, D., Katti, D. S., & Mehrotra, D. (2020). Polycaprolactone as biomaterial for bone scaffolds: Review of literature. *Journal of Oral Biology and Craniofacial Research, 10*(1), 381-388. [DOI:10.1016/j.jobcr.2019.10.003] [PMID] [PMCID]

Frohbergh, M. E., Katsman, A., Mondrinos, M. J., Stabler, C. T., Hankenson, K. D., Oristaglio, J. T., & Lelkes, P. I. (2015). Osseointegrative properties of electrospun hydroxyapatite-containing nanofibrous chitosan scaffolds. *Tissue Engineering Part A, 21*(5-6), 970-981. [DOI:10.1089/ten.tea.2013.0789] [PMID] [PMCID]

Hanemann, T. (2008). Influence of particle properties on the viscosity of polymer-alumina composites. *Ceramics International, 34*(8), 2099-2105. [DOI:10.1016/j.ceramint.2007.08.007.]

Hassanajili, S., Karami-Pour, A., Oryan, A., & Talaei-Khozani, T. (2019). Preparation and characterization of PLA/PCL/HA composite scaffolds using indirect 3D printing for bone tissue engineering. *Materials Science and Engineering: C, 104*, 109960. [DOI:10.1016/j.msec.2019.109960.] [PMID]

Jang, E. S., Park, J. W., Kweon, H., Lee, K. G., Kang, S. W., Baek, D. H., ... & Kim, S. G. (2010). Restoration of peri-implant defects in immediate implant installations by Choukroun platelet-rich fibrin and silk fibroin powder combination graft. *Oral Surgery, Oral Medicine, Oral Pathology, Oral Radiology, and Endodontology, 109*(6), 831-836. [DOI:10.1016/j.tripleo.2009.10.038] [PMID]

Kattimani, V. S., Kondaka, S., & Lingamaneni, K. P. (2016). Hydroxyapatite-Past, present, and future in bone regeneration. *Bone and Tissue Regeneration Insights, 7*, BTRI-S36138. [DOI:10.4137%2FBTRI.S36138.]

Liu, D., Zhang, J., Li, Y., Wang, S., & Yang, M. (2012). The effects of Ce on the proliferation, osteogenic differentiation and mineralization function of MC3T3-E1 cells in vitro. *Biological Trace Element Research, 149*(2), 291-297. [DOI:10.1007/s12011-012-9423-8] [PMID]

Ma, M. X., Liu, Q., Ye, C., Grottkau, B., Guo, B., & Song, Y. F. (2017). Preparation of P3HB4HB/(Gelatin+PVA) composite scaffolds by coaxial electrospinning and its biocompatibility evaluation. *BioMed Research International*, 2017. [DOI:10.1155/2017/9251806] [PMID] [PMCID]

Maia, F. R., Bastos, A. R., Oliveira, J. M., Correlo, V. M., & Reis, R. L. (2022). Recent approaches towards bone tissue engineering. *Bone, 154*, 116256. [DOI:10.1016/j.bone.2021.116256] [PMID]

Maruyama, Z., Yoshida, C. A., Furuichi, T., Amizuka, N., Ito, M., Fukuyama, R., ... & Komori, T. (2007). Runx2 determines bone maturity and turnover rate in postnatal bone development and is involved in bone loss in estrogen deficiency. *Developmental dynamics: an official publication of the American Association of Anatomists, 236*(7), 1876-1890. [DOI:10.1002/dvdy.21187] [PMID]

Mazor, Z., Horowitz, R. A., Del Corso, M., Prasad, H. S., Rohrer, M. D., & Dohan Ehrenfest, D. M. (2009). Sinus floor augmentation with simultaneous implant placement using Choukroun's platelet-rich fibrin as the sole grafting material: a radiologic and histologic study at 6 months. *Journal of Periodontology, 80*(12), 2056-2064. [DOI:10.1902/jop.2009.090252] [PMID]

Mojahedian, M., Fahimipour, F., Larsen, K. L., Kalantar, M., Bastami, F., & Omatali, N. (2016). Ethanol-based sol-gel synthesis of nano-crystalline hydroxyapatite with different calcium phosphorus ratios (Ca/P). *Journal of Ceramic Processing Research, 17*(11), 1138-1142.

Ralston, S. H. (2021). Bone structure and metabolism. *Medicine*, *49*(9), 567-571. [DOI:10.1016/j.mpmed.2021.06.009]

Ramesh, N., Ratnayake, J. T., Moratti, S. C., & Dias, G. J. (2020). Effect of chitosan infiltration on hydroxyapatite scaffolds derived from New Zealand bovine cancellous bones for bone regeneration. *International Journal of Biological Macromolecules, 160*, 1009-1020. [DOI:10.1016/j.ijbiomac.2020.05.269] [PMID]

Rastegar, A., Mahmoodi, M., Mirjalili, M., & Nasirizadeh, N. (2021). Platelet-rich fibrin-loaded PCL/chitosan core-shell fibers scaffold for enhanced osteogenic differentiation of mesenchymal stem cells. *Carbohydrate Polymers*, *269*, 118351. [DOI:10.1016/j.carbpol.2021.118351] [PMID]

Sahebalzamani, M. A., Khorasani, M. T., & Joupari, M. D. (2017). Enhancement of fibroblasts outgrowth onto polycaprolactone nanofibrous grafted by laminin protein using carbon dioxide plasma treatment. *Nano Biomedicine Engineering*, *9*(3), 191-198. [DOI:10.5101/nbe.v9i3.p191-198]

Salmoria, G. V., Fancello, E. A., Roesler, C. R., & Dabbas, F. (2013). Functional graded scaffold of HDPE/HA prepared by selective laser sintering: microstructure and mechanical properties. *The International Journal*

of Advanced Manufacturing Technology, 65(9-12), 1529-1534. [DOI:10.1007/s00170-012-4277-y]

Shalumon, K. T., Anulekha, K. H., Chennazhi, K. P., Tamura, H., Nair, S. V., & Jayakumar, R. (2011). Fabrication of chitosan/poly (caprolactone) nanofibrous scaffold for bone and skin tissue engineering. Inte*rnational Journal of Biological Macromolecules, 48*(4), 571-576. [DOI:10.1016/j.ijbiomac.2011.01.020] [PMID]

Shim, J. H., Huh, J. B., Park, J. Y., Jeon, Y. C., Kang, S. S., Kim, J. Y., ... & Cho, D. W. (2013). Fabrication of blended polycaprolactone/poly (lactic-co-glycolic acid)/β-tricalcium phosphate thin membrane using solid freeform fabrication technology for guided bone regeneration. *Tissue Engineering Part A, 19*(3-4), 317-328. [DOI:10.1089/ten.tea.2011.0730] [PMID] [PMCID]

Shor, L., Güçeri, S., Wen, X., Gandhi, M., & Sun, W. (2007). Fabrication of three-dimensional polycaprolactone/hydroxyapatite tissue scaffolds and osteoblast-scaffold interactions in vitro. *Biomaterials, 28*(35), 5291-5297. [DOI:10.1016/j.biomaterials.2007.08.018] [PMID]

Shrivats, A. R., McDermott, M. C., & Hollinger, J. O. (2014). Bone tissue engineering: state of the :union: *Drug Discovery Today, 19*(6), 781-786. [DOI:10.1016/j.drudis.2014.04.010] [PMID]

Simonpieri, A., Del Corso, M., Sammartino, G., & Ehrenfest, D. M. D. (2009). The relevance of Choukroun's platelet-rich fibrin and metronidazole during complex maxillary rehabilitations using bone allograft. Part I: a new grafting protocol. *Implant Dentistry, 18*(2), 102-111. [DOI:10.1097/ID.0b013e318198cf00] [PMID]

Souza, E. Q. M., Klaus, A. E. C., Santos, B. F. E., da Costa, M. C., Ervolino, E., de Lima, D. C., & Fernandes, L. A. (2020). Evaluations of hydroxyapatite and bioactive glass in the repair of critical size bone defects in rat calvaria. *Journal of Oral Biology and Craniofacial Research, 10*(4), 422-429. [DOI:10.1016/j.jobcr.2020.07.014] [PMID] [PMCID]

Tian, B., Wang, N., Jiang, Q., Tian, L., Hu, L., & Zhang, Z. (2021). The immunogenic reaction and bone defect repair function of ε-poly-L-lysine (EPL)-coated nanoscale PCL/HA scaffold in rabbit calvarial bone defect. *Journal of Materials Science: Materials in Medicine, 32*(6), 1-12. [DOI:10.1007/s10856-021-06533-7] [PMID] [PMCID]

Tian, L., Zhang, Z., Tian, B., Zhang, X., & Wang, N. (2020). Study on antibacterial properties and cytocompatibility of EPL coated 3D printed PCL/HA composite scaffolds. *RSC Advances, 10*(8), 4805-4816. [DOI:10.1039/C9RA10275B] [PMID] [PMCID]

Turnbull, G., Clarke, J., Picard, F., Riches, P., Jia, L., Han, F., ... & Shu, W. (2018). 3D bioactive composite scaffolds for bone tissue engineering. *Bioactive Materials*, *3*(3), 278-314. [DOI:10.1016/j.bioactmat.2017.10.001] [PMID] [PMCID]

Venugopal, E., Sahanand, K. S., Bhattacharyya, A., & Rajendran, S. (2019). Electrospun PCL nanofibers blended with Wattakaka volubilis active phytochemicals for bone and cartilage tissue engineering. *Nanomedicine: Nanotechnology, Biology and Medicine*, *21*, 102044. [DOI:10.1016/j.nano.2019.102044] [PMID]

Wall, I., Donos, N., Carlqvist, K., Jones, F., & Brett, P. (2009). Modified titanium surfaces promote accelerated osteogenic differentiation of mesenchymal stromal cells in vitro. *Bone, 45*(1), 17-26. [DOI:10.1016/j.bone.2009.03.662] [PMID]

Wei, J., Yoshinari, M., Takemoto, S., Hattori, M., Kawada, E., Liu, B., & Oda, Y. (2007). Adhesion of mouse fibroblasts on hexamethyldisiloxane surfaces with wide range of wettability. *Journal of Biomedical Materials Research Part B: Applied Biomaterials: An Official Journal of The Society for Biomaterials, The Japanese Society for Biomaterials, and The Australian Society for Biomaterials and the Korean Society for Biomaterials*, *81*(1), 66-75. [DOI:10.1002/jbmb. PMID: 16924616.] [PMID]

Yang, M., Zhu, S., Chen, Y., Chang, Z., Chen, G., Gong, Y., ... & Zhang, X. (2004). Studies on bone marrow stromal cells affinity of poly (3-hydroxybutyrate-co-3-hydroxyhexanoate). *Biomaterials, 25*(7-8), 1365-1373. [DOI:10.1016/j.biomaterials.2003.08.018] [PMID].

Iranian Journal of Veterinary Medicine
Abstracts in Persian Language
Online ISSN 2252-0554
10.22059/IJVM.2022.335899.1005219
مجله طب دامی ایران، ۱۴۰۱، دوره ۱۶، شماره ۴، ۴۱۳-۴۰۰

ساخت داربست‌های پرینت سه‌بعدی پلی کاپرولاکتون/هیدروکسی آپاتیت با پوشش فیبرین غنی از پلاکت (PCL-HA/PRF) برای مهندسی بافت استخوان

سینا یل بیرانوند[1]، حسین نورانی[2]، حسین کاظمی مهرجردی[1*]

[1] گروه علوم درمانگاهی، دانشکده دامپزشکی، دانشگاه فردوسی مشهد، مشهد، ایران
[2] گروه پاتوبیولوژی، دانشکده دامپزشکی، دانشگاه فردوسی مشهد، مشهد، ایران

(دریافت مقاله: ۲۸ آذر ماه ۱۴۰۰، پذیرش نهایی: ۲۳ اسفند ۱۴۰۰)

زمینه مطالعه: مهندسی بافت یک استراتژی امیدوارکننده برای ترمیم نقایص بافت استخوانی است. علاوه بر این، فناوری چاپ سه‌بعدی مزایای قابل توجهی در تولید داربست‌های مهندسی زیستی برای درمان نقایص استخوانی منحصربه‌فرد برای هر بیمار ارائه می‌دهد

هدف: هدف از این مطالعه، سنتز و بررسی خواص داربست‌های چاپ سه بعدی پلی کاپرولاکتون/هیدروکسی آپاتیت (PCL-HA) اصلاح شده با فیبرین غنی از پلاکت (PRF) است.

روش کار: داربست‌ها با استفاده از فناوری چاپ سه‌بعدی برای ایجاد محیطی مناسب برای بازسازی استخوان ساخته شدند. میکروسکوپ الکترونی روبشی (SEM)، تبدیل فوریه فروسر (FT-IR)، و تست‌های مکانیکی فشاری برای مشخص کردن مورفولوژی، ریزساختار و خواص مکانیکی داربست به کار گرفته شد. قابلیت چسبندگی سلولی، تکثیر، زیست سازگاری و تمایز نیز بررسی شد.

نتایج: در نتیجه افزودن نانوذرات هیدروکسی آپاتیت (HA)، داربست‌های PCL-HA چاپ سه‌بعدی با منافذ به هم پیوسته سطح ناهموار و خواص مکانیکی بهبود یافته داشتند. به دلیل آب دوستی و تخلخل بالاتر داربست PCL-HA/PRF در مقایسه با داربست PCL، رشد سلول‌های استخوانی در سطح داربست PCL-HA/PRF مشاهده شد. نتایج سنجش سمیت سلولی به‌طور قابل‌توجهی سازگاری سلولی داربست‌های PCL-HA/PRF را نسبت به داربست‌های PCL و PCL-HA نشان داد.

نتیجه‌گیری نهایی: نتایج نشان می‌دهد که داربست‌های چاپ سه بعدی PCL-HA اصلاح شده با فیبرین غنی از پلاکت (PRF) می‌توانند در بازسازی بافت استخوانی مؤثر باشند.

واژه‌های کلیدی: داربست‌های چاپ سه‌بعدی، مهندسی بافت استخوان، هیدروکسی آپاتیت، تمایز استخوانی، فیبرین غنی از پلاکت

نویسندهٔ مسئول: حسین کاظمی مهرجردی، گروه علوم درمانگاهی، دانشکده دامپزشکی، دانشگاه فردوسی مشهد، مشهد، ایران ، ایران
ایمیل: h-kazemi@um.ac.ir